Separation and Purification Technology 374 (2025) 133634

Contents lists available at ScienceDirect

Separation and Purification Technology

journal homepage: www.elsevier.com/locate/seppur

Activation of persulfate by biochar and iron: role of biochar pyrolysis conditions and ash amendments

Yiling Zhuang [a,b,1], Stefan B. Haderlein [b], Nikolas Hagemann [c,d], Jannis Grafmüller [d,e], Karolin Gogler [b], Andrea Paul [f], Friedrich Fink [f], Stephanie Spahr [a,*]

[a] Department of Ecohydrology and Biogeochemistry, Leibniz Institute of Freshwater Ecology and Inland Fisheries (IGB), Müggelseedamm 301, 12587 Berlin, Germany
[b] Department of Geosciences, Environmental Mineralogy and Chemistry, Eberhard Karls University of Tübingen, Schnarrenbergstr. 94-96, 72076 Tübingen, Germany
[c] Environmental Analytics, Agroscope, Reckenholzstrasse 191, 8046 Zürich, Switzerland
[d] Ithaka Institut gGmbH, Altmutterweg 21, 63773 Goldbach, Germany
[e] Institute of Sustainable Energy Systems (INES), Offenburg University of Applied Sciences, 77652 Offenburg, Germany
[f] Bundesanstalt für Materialforschung und –prüfung (BAM), Richard-Willstätter-Straße 11, 12489 Berlin, Germany

ARTICLE INFO

Keywords:
Fenton-like systems
Oxidation processes
Water treatment
Pyrogenic carbon
Redox-active moieties
Electron donating capacity
Persistent free radicals

ABSTRACT

Redox-active biochars can enhance contaminant transformation in persulfate-based Fenton-like water treatment by facilitating Fe(III) reduction to Fe(II). However, biochar properties vary greatly depending on both feedstock selection and pyrolysis conditions. Best suited biochars for Fe(III) reduction and persulfate activation have yet to be identified. Here, we investigated eight biochars for their ability to activate persulfate with Fe(III) to transform *N,N*-diethyl-*m*-toluamide (DEET) in water. Four of the biochars were produced from beech wood under different pyrolysis conditions (450–750 °C, high and low nitrogen flow rate in the reactor) and four biochars were produced from softwood amended with 0 – 43 weight percent (wt%) wood ash prior to pyrolysis at 500 °C. Beech wood biochar produced at 450 °C transformed DEET most efficiently with a half-life time of 39 ± 4 min, likely due to the high concentration of surface oxygen functional groups and persistent free radicals that accelerated Fe(III) reduction and formation of reactive species. Among the ash-amended biochars, biochar with 16 wt% ash amendment showed the most efficient DEET transformation with a half-life time of 27 ± 0.6 min, which is 10-times faster compared to a non-ash-amended biochar produced from the same biomass under similar pyrolysis conditions. Ash amendment led to the formation of crystalline iron minerals in biochars, which likely promoted Fe(III) reduction and persulfate activation. Our results highlight the potential for fine-tuning the redox properties of biochar, e.g., by ash amendment to a woody feedstock, enabling tailored performance for specific water treatment applications.

1. Introduction

Fenton-like processes using peroxydisulfate ($S_2O_8^{2-}$, PDS) for oxidative water treatment and contaminant removal have gained much attention for environmental applications [1–3]. However, the oxidation efficiency of the Fe(II)/PDS system is limited by the sluggish Fe(III)/Fe(II) cycling and Fe(III) precipitation [4–6]. The PDS-based Fenton-like system can be enhanced by the addition of redox-active biochars [7–9]. Biochars can enhance the reduction of Fe(III) to Fe(II), which activates PDS to reactive species for the removal of organic contaminants [9–14]. The performance of different biochars for Fe(III) reduction and PDS activation highly depends on its redox-active properties, especially the electron donating capacity (EDC) [15,16]. Redox-active moieties in biochar include surface functional groups, persistent free radicals (PFRs), metals like iron and manganese oxides embedded in the carbonaceous matrix, and conjugated aromatic structures [17–19]. Surface functional groups, e.g. quinone and phenolic groups, are abundant and are the major moieties contributing to EDC [20–22]. They promote electron transfer through charging-discharging cycles where biochar acts as a "battery" [23]. Polycyclic aromatic compounds with conjugated π-electron systems make biochar electrically conductive and were proposed to also have a contribution to EDC [24,25]. Biochars with high

* Corresponding author.
E-mail address: stephanie.spahr@igb-berlin.de (S. Spahr).
[1] Present address: School of Environmental Science & Engineering, Xiamen University of Technology, Xiamen, 361024, China.

https://doi.org/10.1016/j.seppur.2025.133634
Received 13 February 2025; Received in revised form 29 April 2025; Accepted 18 May 2025
Available online 20 May 2025

bulk electrical conductivity may function as an "electrical conduit" that can undergo direct electron transfer through carbon matrices [23]. The nature and abundance of redox-active moieties in biochars can thus affect the mechanism and efficiency of Fe(III) reduction and PDS activation in the biochar/Fe(III)/PDS system.

The nature and abundance of the redox-active moieties in biochars is influenced by both the selection of feedstock and the pyrolysis conditions applied [26,27]. While functional groups on biochar tend to diminish with increasing pyrolysis temperature, the degree of aromatic compound conjugation (the "aromaticity") simultaneously increases [28,29]. This complex interplay makes it difficult to predict the optimal pyrolysis conditions that would provide a biochar with the greatest potential to activate PDS. Furthermore, the term pyrolysis conditions encompasses a variety of factors beyond temperature, such as residence time and gas flow in the reactor, all of which can significantly affect the biochar properties [30].

The impact of pyrolysis temperature on the biochar performance and reactive species formation in the biochar/Fe(III)/PDS system has been investigated [10,14]. Liang et al. 2021 found a fast Fe(III)/Fe(II) cycling and an Fe(IV)-dominated pathway when using biochar produced at 400 °C [14]. In contrast, high-temperature biochars produced at 700 °C could not maintain the Fe(III)/Fe(II) cycling and the contaminant transformation was governed by a mediated electron transfer from organics to persulfate by biochar [14]. Tang et al. 2023 reported that the biochar/Fe(III)/PDS system exhibited the greatest performance in organic contaminant transformation at 500 °C (range tested: 350 – 700 °C), accompanied by the highest contribution of radical species [10]. Meanwhile, the nonradical contribution of Fe(IV) increased with decreasing pyrolysis temperature from 700 °C to 350 °C [10]. However, little is known about the role of other biochar pyrolysis conditions and the resulting redox-active moieties for the performance of biochars in PDS activation and organic contaminant transformation in the biochar/Fe(III)/PDS system.

Feedstock treatments prior to pyrolysis may include mixing additives such as wood ash with biomass to manipulate the redox-active properties of the resulting biochar [31–33]. Wood ash, a by-product of biomass power plants, is particularly beneficial for modifying the redox-active properties of biochar due to its high mineral content and pH buffering capacity [31,34]. Ash-amended biochars have shown improved performance for agricultural crop production [32,33] and the removal of inorganic contaminants such as heavy metals from water [31]. Ash-amended biochars have also been reported to possess enhanced redox properties with both higher electron donating and electron accepting capacity [33], which bears potential for application in the biochar/Fe(III)/PDS system. However, to the best of our knowledge, ash-amended biochars have not yet been tested for organic contaminant transformation in Fenton-like PDS-based oxidation processes for water treatment.

Therefore, the objectives of this work were (i) to investigate the effects of pyrolysis conditions, specifically pyrolysis temperature, gas flow, and feedstock treatment (ash amendment to woody feedstock) on organic contaminant transformation in the biochar/Fe(III)/PDS system and (ii) to gain insights into the role of redox-active moieties of biochar for Fe(III) reduction and PDS activation. To this end, we performed laboratory batch experiments with biochars produced under different pyrolysis conditions and studied the transformation kinetics of the insect repellent *N,N*-diethyl-*m*-toluamide (DEET) as our model compound, for which we recently demonstrated transformation upon activation of PDS in the presence of Fe(III) at pH 2.5 [11]. We evaluated the performance of the different biochars for DEET removal in the biochar/Fe(III)/PDS system with respect to the biochar characteristics, particularly the redox properties and redox-active moieties.

2. Materials and methods

A list of all chemicals including suppliers and purities is provided in Section S1 of the Supporting Information.

2.1. Biochar preparation

The pyrolysis of the biochars was performed in a continuously operating auger reactor on pilot-plant scale (PYREKA, Pyreg GmbH, Dörth, Germany), as described in Hagemann et al., 2020 [35]. If not mentioned otherwise, the reactor was purged with N_2 at a flow rate of 2 L min $^{-1}$ and biochars were produced with a residence time of the solids in the reactor of 10 min. Four biochars were produced from beech wood (milled and sieved to 2 – 6 mm, Verora AG, Edlibach, Switzerland) at three different temperatures (450°C, 600°C, and 750°C). One biochar was produced at 450 °C with a higher N_2 flow rate of 10 L min $^{-1}$. In the following, these beech wood biochars are referred to as BC450, BC450HF ("high flow"), BC600, and BC750. To study the impact of ash amendments, four biochars were produced at 500 °C from softwood sawdust (Allspan Spanverarbeitung GmbH, Karlsruhe, Germany) to which wood ash (bottom ash sampled in a combustion plant in Sissach, Switzerland provided by Holz & Forst Consulting GmbH, Binningen, Switzerland, dry matter basis) was added prior to pelleting and subsequent pyrolysis. For the elemental composition of the wood ash see Table S3. Wood ash has been reported to be rich in Ca, Si, K, Mg, P, Mn and Fe, with Fe content ranging from 2 – 5 % depending on the feedstock and combustion conditions [36,37]. Different amounts of ash (0, 8.9, 16.4, and 42.6 weight percent (wt %)) were amended prior to pelleting and subsequent pyrolysis as described in Grafmüller et al., 2022 [33], resulting in biochars with an actual ash content of 2.3 %, 24.4 %, 41.1 %, and 69.0 %, respectively. The four softwood sawdust ash-amended biochars are referred to as BC-ash0 ("biochar with 0 wt% ash additive"), BC-ash9, BC-ash16, and BC-ash43. All biochars were ground using an impact mill (Kinematica AG, Lucerne, Switzerland) to a particle size of < 200 μm (Fig. S1) and kept in a desiccator until further use.

2.2. Batch experiments with biochar, Fe(III), and PDS

Batch experiments were conducted in 40 mL amber glass vials at room temperature on an overhead shaker. A 1 g L^{-1} biochar suspension was prepared with 30 mg biochar in 30 mL deionized water and the initial pH was adjusted to 2.5 with 0.25 M H_2SO_4. *N,N*-diethyl-*m*-toluamide (DEET) was added to the biochar suspension from an aqueous 10 mM stock solution to achieve a nominal initial concentration of 50 μM DEET. For experiments with BC750, a nominal initial concentration of 100 μM was used due to the high adsorption capacity of BC750 (Fig. S4). After 30 min contact time, an apparent sorption equilibrium was reached (Fig. S4). Subsequently, the reaction was initiated by adding 60 μL of Fe(III) from a 0.05 M aqueous Fe(III) sulfate stock solution to reach an initial concentration of 0.2 mM Fe(III), followed by adding 240 μL of PDS from a 1 M aqueous stock solution to obtain an initial nominal PDS concentration of 8 mM. At pre-defined time points, 1 mL aliquots were sampled and immediately added into a mixture of 100 μL methanol (2 M in the sample, ≈ 9 % v/v) and 5.5 μL NaOH (10 mM in the sample, ≈ 1 % v/v, pH > 11) to quench the reaction and precipitate iron. Samples were filtered through 0.22 μm syringe filters (PES, BGB Analytik, Germany; 88.5 ± 0.7 % DEET recovery) and kept in glass vials for DEET analysis, which was not affected by methanol nor by NaOH addition. The pH was monitored and controlled at 2.5 ± 0.1 by adding small amounts H_2SO_4 or NaOH during the reaction. Control experiments containing DEET and either biochar, Fe(III), or PDS only, and combinations thereof were performed as described above.

2.3. Quantification of biochar-induced Fe(III) reduction

To evaluate the Fe(III) reduction potential of the biochars, 1 g L^{-1} biochar suspensions were spiked with 0.1 mM Fe(III) sulfate to reach 0.2 mM Fe(III) and the dissolved Fe(II) concentrations were determined over a two-hour period using a modified Ferrozine assay, adapted from

the protocols of Stookey et al., 1970 [38] and Amstaetter et al., 2012 [39]. In this procedure, filtered aliquots of each sample were immediately added to 1 M HCl in disposable 1.5 mL cuvettes (BrandTech) to stabilize Fe(II) and prevent oxidation. The Ferrozine reagent was added, forming a purple Fe^{2+} complex, which was quantified spectrophotometrically at 562 nm after 5-minute incubation in the dark.

2.4. Biochar characterization

2.4.1. Electron exchange capacity (EEC)

The electron exchange capacity (EEC) was determined using a mediated electrochemical reduction (MER) and mediated electrochemical oxidation (MEO) method adopted from Klüpfel et al., 2014 [24]. All analyses were conducted in a glovebox under N_2 atmosphere to maintain anoxic conditions. The biochars were placed under vacuum in the antechamber overnight to remove adsorbed O_2 and then transferred into the glovebox to prepare a 10 g L^{-1} biochar suspension in anoxic deionized water. The biochar suspensions were stirred for at least 24 h to ensure complete dispersion before analysis. For the electrochemical setup and measurement details see Section S2. The electron accepting capacity (EAC) and electron donating capacity (EDC) were calculated in μmol e^- (g biochar)$^{-1}$ according to Klüpfel et al., 2014 [24].

2.4.2. Solid-state electrical conductivity

The solid-state electrical conductivity (here called: SEC) of the biochars was determined using a "Black Gauß" electrical cell (Eurofins Umwelt Ost GmbH, Freiberg, Germany) and a hydraulic press (Perkin Elmer GmbH, Überlingen, Germany) according to the manufacture's manual [40]. Biochar samples were sequentially compressed with a pressure of 30, 60, 90, 130 and 160 MPa in the measurement cell.

2.4.3. Persistent free radicals

Persistent free radicals (PFRs) were determined by continuous wave X-band electron spin resonance (ESR) spectroscopy (MiniScope MS 300, Magnettech GmbH, Berlin, Germany). The spectra were accumulated 3-fold over 90 s at a microwave power of 0.1 mW (sweep width 15 mT) and Suwannee River standard fulvic acid (1S101F, IHSS) was used as a reference with a free radical content of 0.54 x 10^{17} spins g^{-1} for the calculation of spin concentrations. The g-values were determined in separate scans by measuring a certified internal manganese standard (Mn^{2+} in ZnS) simultaneously with the samples. Both PFRs and g-values were determined in duplicate.

2.4.4. Size distribution, elemental composition, and surface area

The biochar size distribution was determined by a Mastersizer 2000 (Malvern Inc., UK). The elemental composition as well as the ash and water contents of the beech wood biochars were analyzed at Eurofins (Freiberg, Germany) according to the analytical guidelines of the European Biochar Certificate (EBC 2012–2023) [41]. The specific surface area of the beech wood biochars was determined in N_2 physisorption experiments at 77 K and sorption isotherms were modelled using the Brunauer–Emmett–Teller (BET) method (Section S2). For the analysis of ash-amended biochars, see Table S3 and Grafmüller et al., 2022 [33].

2.4.5. Surface functional groups and metal content

The functional groups on the biochar surface were characterized by attenuated total reflectance Fourier transform infrared (ATR-FTIR) spectroscopy. The spectra were recorded using a Nicolet 670 FT-IR spectrometer (Thermo Fisher Scientific GmbH) equipped with an Ever-Glo source, a KBr beam splitter, and a deuterated L-alanine-doped triglycene sulphate (DLaTGS) detector. In situ X-ray diffraction analysis (XRD) measurements were performed for the investigation of biochar surface structure properties on a Bruker D2 PHASER X-ray diffractometer. The metal content of the biochars was determined by inductively coupled plasma-optical emission spectroscopy (ICP-OES, ICP iCAP 7000 series, Thermo Fisher Scientific Inc.) after microwave acid digestion. For detailed information of the biochar characterization see Section S2.

2.5. DEET quantification

The concentration of DEET in aqueous solutions was quantified by high-performance liquid chromatography equipped with a diode array detector (HPLC UV–vis, 1200 Series, Agilent, USA). The wavelength was set to 210 nm. 10 μL of sample was injected and analyzed with a C18 column (150 mm × 4.6 mm, 5 μm, ZORBAX Eclipse XDB-C18, Agilent). The eluent mixture consisted of 60 % methanol and 40 % water (pH 3, 1 mM H_2SO_4) at a flow rate of 0.5 mL min^{-1}. DEET concentrations were quantified by external calibration from 2 to 200 μM.

2.6. Data analysis

Pseudo-first order rate constants (k_{obs}) and half-life times ($t_{1/2}$) were calculated according to eq. (1) and eq. (2), respectively:

$$\ln\frac{c_t}{c_0} = -k_{obs} \bullet t \quad (1)$$

$$t_{1/2} = \frac{\ln 2}{k_{obs}} \quad (2)$$

where c_t is the concentration of DEET at time t and c_0 is the measured initial DEET concentration in the biochar suspension after 30 min sorption equilibrium.

3. Results and discussion

3.1. Impact of biochar pyrolysis temperature on DEET transformation in the presence of Fe(III) and persulfate (PDS)

3.1.1. Performance of beech wood biochars

As shown in Fig. 1a, DEET was transformed most efficiently with the two low-temperature biochars BC450 and BC450HF in the biochar/Fe(III)/PDS system. BC450 resulted in 88 ± 3 % DEET transformation within two hours following pseudo-first order kinetics with a k_{obs} of (2.9 ± 0.1) × 10^{-4} s^{-1} (Fig. S6) and a $t_{1/2}$ of 39 ± 4 min. The k_{obs} for DEET transformation in the BC450HF/Fe(III)/PDS system was (2.2 ± 0.1) × 10^{-4} s^{-1} and only slightly lower than the one obtained with BC450/Fe(III)/PDS (Fig. S6). The N_2 flow rate during feedstock pyrolysis thus had a minor effect on the performance of the biochars, which is reflected in similar biochar properties (Table S2).

In contrast, the pyrolysis temperature had a significant effect on the biochar properties and DEET transformation. When BC600 was employed together with Fe(III) and PDS, 31 ± 1 % of DEET was transformed and the $t_{1/2}$ of DEET was 227 ± 9 min with a k_{obs} of (0.4 ± 0.1) × 10^{-4} s^{-1} (Fig. S6). The latter is 7.3 times lower than the k_{obs} in the BC450/Fe(III)/PDS system. Experiments with BC750 did not lead to DEET transformation (Fig. 1a). On the contrary, we observed a sharp increase in aqueous DEET concentration after PDS addition, indicating desorption of DEET from BC750 rather than transformation (Fig. S6). Decreasing DEET reaction rate constants with increasing pyrolysis temperatures suggest distinctly different biochar properties affecting PDS activation. In control batches with PDS only, biochar only, Fe(III) only, and combinations thereof, DEET removal was much less efficient (< 5.5 – 29 %, Fig. S5). The accelerated DEET transformation in the low-temperature biochar/Fe(III)/PDS systems indicates biochar-mediated Fe(III) reduction leading to continuous PDS activation upon reaction with Fe(II) as shown in our previous and other studies [9–12,14].

3.1.2. Redox-active properties of beech wood biochars

All beech wood biochars possessed an electron donating capacity (EDC, Fig. 1b) and were able to reduce Fe(III) to Fe(II) (Fig. 1c). EDC was highest for BC750 (529 ± 42 μmol e^- (g biochar)$^{-1}$), followed by BC450 and BC450HF (413 ± 22 and 413 ± 23 μmol e^- (g biochar)$^{-1}$,

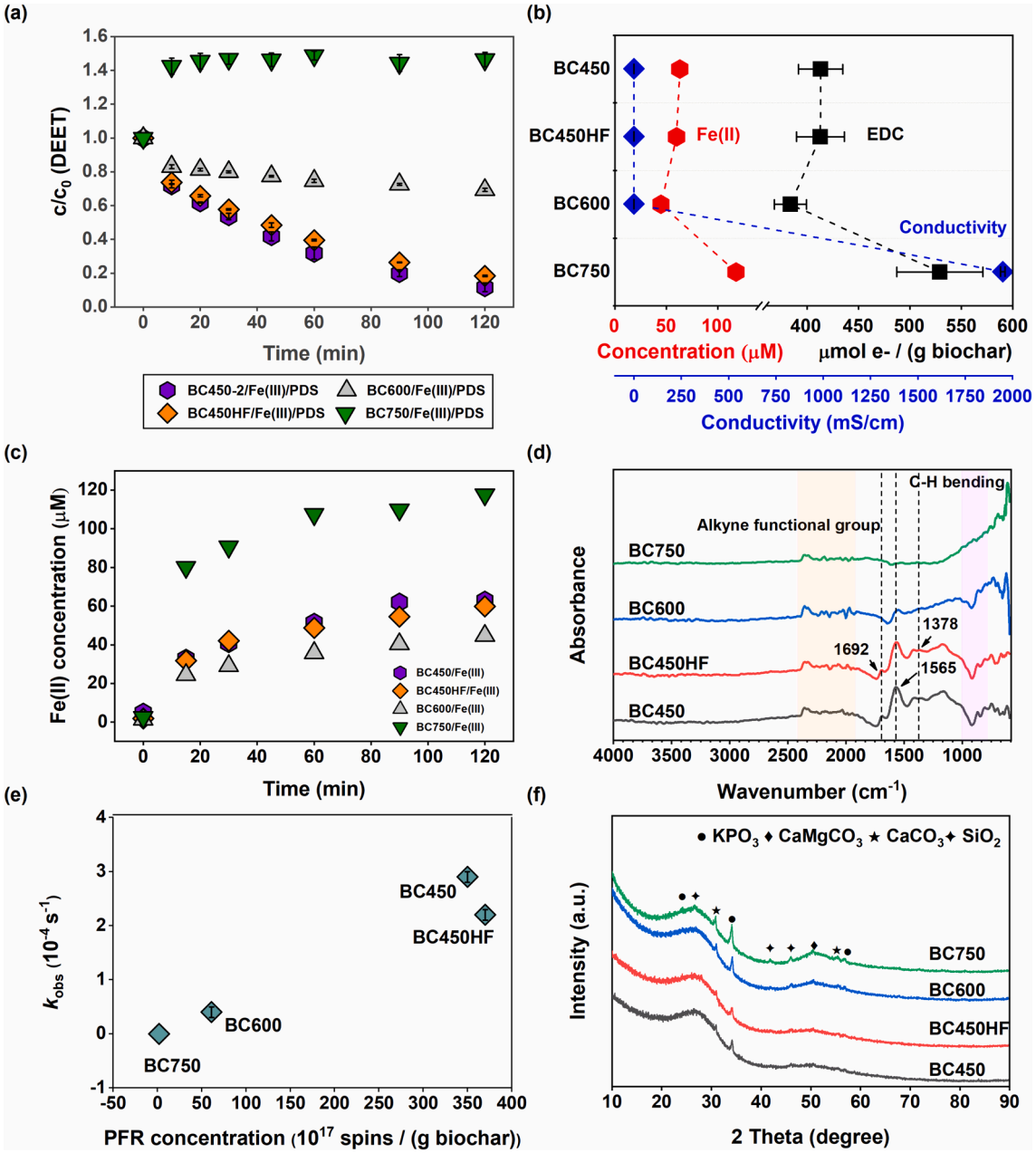

Fig. 1. (a) Kinetics of DEET transformation in the biochar/Fe(III)/PDS system with beech wood biochars pyrolyzed at different conditions (BC450, BC450HF, BC600, and BC750). [Biochar] = 1 g L^{-1}, [Fe(III)] = 0.2 mM, [PDS] = 8 mM, c_0 = measured DEET concentration after sorption equilibrium (~ 40 μM), c = measured DEET concentration over time, pH 2.5. (b) Electron donating capacity (EDC, E_h (MEO) = 0.61 V) and solid-state electrical conductivity (SEC, pressure 160 MPa) of the biochars, and corresponding Fe(II) formation after 120 min in biochar suspensions spiked with Fe(III). [Biochar] = 1 g L^{-1}, [Fe(III)] = 0.2 mM, pH 2.5. (c) Fe(II) formation in biochar suspensions spiked with Fe(III). [Biochar] = 1 g L^{-1}, [Fe(III)] = 0.2 mM, pH 2.5. (d) ATR-FTIR spectra (similar water contents, see Table S2). (e) Persistent free radical (PFR) concentrations of the biochars and DEET transformation rate constants (k_{obs}) derived from (a). (f) X-ray diffraction (XRD) spectra of the beech wood biochars BC450, BC450HF, BC600 and BC750. Error bars indicate the standard deviation of triplicate experiments.

respectively), and BC600 (384 ± 16 μmol e^- (g biochar)$^{-1}$) (Fig. 1b, Table S2). These values are consistent with findings from previous studies [18,24] and highlight the strong influence of pyrolysis temperature on the EDC of biochars. Yet, the EDC values cannot explain the observed differences in DEET transformation in the biochar/Fe(III)/PDS system, suggesting that specific biochar characteristics, particularly the type of redox-active functional groups and structural properties, govern PDS activation and DEET transformation. In fact, we observed major differences in the redox-active moieties of the biochars, where biochars produced at pyrolysis temperatures ≤ 600 °C contained oxygen functional groups and persistent free radicals (PFRs), which likely promote PDS activation and DEET transformation. In contrast, biochar produced at 750 °C consisted of conductive graphene-like structures resulting in a high EDC value but no DEET transformation in the presence of Fe(III) and PDS.

The contribution of oxygen-containing functional groups to the EDC of BC450, BC450HF, and BC600 is supported by FTIR analyses, which revealed peaks corresponding to C=O conjugated ketones (1692 cm^{-1}), –COOH (1565 cm^{-1}), and phenolic-OH (1378 cm^{-1}) [42] (Fig. 1d). These functional groups, which can participate in electron transfer reactions, decreased in intensity with increasing pyrolysis temperature. Notably, no redox-active functional groups were detected in biochar produced at 750 °C (Fig. 1d).

PFRs, which are organic moieties with unpaired electrons, also

contribute to the EDC of biochars [20,43]. The g-values of all biochars were < 2.0030 indicating the presence of carbon-centered PFRs [44], which can form during pyrolysis from hemicellulose, cellulose, and lignin precursors [43]. The PFR concentrations decreased as the pyrolysis temperature increased (Table S2), in agreement with previous studies showing PFR elimination on biochar surfaces at pyrolysis temperatures > 700 °C [12,20,45]. BC450 and BC450HF displayed the highest PFR concentrations in the range of $(3.5 \pm 0.4) \times 10^{19}$ spins (g biochar)$^{-1}$, which is two orders of magnitude higher than that of BC750 ($(1.9 \pm 0.1) \times 10^{17}$ spins (g biochar)$^{-1}$) (Fig. 1e, Table S2). These results suggest that lower temperature biochars derive their EDC primarily from oxygenated functional groups and PFRs.

Inorganic redox-active metal species, mainly Fe and Mn, also contribute to the EDC [24], though their role is minor in the biochars produced from beech wood with low mineral content. The concentrations of Fe and Mn increased with increasing pyrolysis temperature due to greater mass loss from volatilization of organic compounds (Table S1). However, the contribution of these metals to the total EDC was low and explained only 1.3 – 2.0 % of the measured EDCs (Table S1). XRD analysis confirmed the absence of redox-active minerals in beech wood biochars (Fig. 1f), indicating that Fe and Mn played a minor role in the redox activity.

Solid-state electrical conductivity (SEC) of the biochars showed a strong correlation with pyrolysis temperature (Fig. 1b, Fig. S3 and Table S2). BC750 demonstrated a nearly eight orders of magnitude greater SEC (1949 ± 12 mS cm^{-1}) than BC450 with an SEC of (7.6 ± 0.3) $\times 10^{-5}$ mS cm^{-1}. Differences in SEC are derived from formation of graphene-like structures at high pyrolysis temperatures with conjugated π-electron systems that facilitate direct electron transfer through the carbon matrix [23,46]. These results, along with the lowest H/C and O/C ratios in BC750 (Table S2), show a high degree of aromatic condensation in BC750 and indicate that the EDC of high-temperature biochars is governed by conductive carbon structures rather than redox-active functional groups.

3.1.3. Impact of redox-active properties of biochars on Fe(III) reduction and DEET transformation

The pyrolysis of beech wood at different temperatures led to biochars with distinctive electrochemical properties that governed the reduction of Fe(III) and DEET transformation in the biochar/Fe(III)/PDS system. All biochars successfully reduced Fe(III) to Fe(II) in aqueous solution, with Fe(II) formation increasing with increasing EDC values of the biochars (Fig. 1b). BC750 led to the highest Fe(II) formation, followed by BC450 and BC450HF, and BC600 (Fig. 1b and Fig. 1c). However, while all biochars possessed an EDC and were able to reduce Fe(III) to Fe(II), DEET was only transformed when employing low pyrolysis temperature biochars (≤600 °C) together with Fe(III) and PDS. These results indicate that oxygen-containing functional groups and PFRs in the BC450, BC450HF, and BC600 play a key role for DEET transformation in the biochar/Fe(III)/PDS system. In fact, a positive correlation was obtained for PFR concentration of the biochars and DEET transformation rate constants (Fig. 1e). BC750, in contrast, contained conductive graphene-like structures that contributed to high EDCs and Fe(III) reduction, but did not support and rather inhibited DEET transformation.

Low-temperature biochars in the biochar/Fe(III)/PDS system initiated an efficient Fe(III)/Fe(II) cycling induced by the high amount of oxygen-containing functional groups and PFRs that may form reactive species leading to DEET transformation. These findings align with our previous study, which demonstrated that sulfate radicals are the dominant reactive species involved in DEET transformation in the BC450/Fe(III)/PDS system [11]. Our results are also consistent with findings of Liang et al., 2021, who reported rapid Fe(III)/Fe(II) cycling due to the conversion between semiquinone radicals and quinones in biochars produced at 400 °C [14]. In contrast, for high-temperature biochars with its high content of conjugated aromatic structures and high SEC, contaminant transformation has been suggested via a nonradical electron transfer pathway [14,23,47,48], in which electron transfer from organics (electron donor) to persulfate (electron acceptor) is mediated by biochar [23]. Nonradical electron transfer processes exhibit high selectivity towards electron-rich organic substances [49], and are therefore not favorable for our model compound DEET.

3.2. Impact of ash amendments in biochar production on DEET transformation in the presence of Fe(III) and PDS

3.2.1. Performance and redox properties of ash-amended softwood sawdust biochars

To investigate the effects of ash amendments on the redox properties and performance of the biochars in the biochar/Fe(III)/PDS system, different amounts of ash (0, 9, 16, 43 wt%) were added to softwood sawdust prior to pelleting and pyrolysis at 500 °C. All ash-amended biochars significantly outperformed the non-ash amended control biochar (BC-ash0) in facilitating DEET transformation in the presence of Fe(III) and PDS (Fig. 2a). The observed DEET transformation rate constants, k_{obs}, of BC-ash9, BC-ash16, and BC-ash43 were 7.25, 10, and 4.5 times higher than the k_{obs} of the BC-ash0, respectively (Fig. 2a and Fig. S7). BC-ash16 led to the most efficient DEET transformation with a k_{obs} of $(4.0 \pm 0.1) \times 10^{-4}$ s^{-1} (Fig. S7). The addition of ash prior to pyrolysis thus seemed to produce biochars with beneficial properties for enhanced PDS activation and contaminant transformation in the presence of Fe(III).

We investigated the ash-amended biochars for their ability to reduce Fe(III) in relation to their EDC values. In biochar suspensions spiked with 0.2 mM of Fe(III), all ash-amended biochars produced significantly higher concentrations of Fe(II) compared to the non-ash amended control biochar (BC-ash0) (Fig. 2b and Fig. 2c). BC-ash16 yielded the highest Fe(II) concentration of 68 μM, followed by BC-ash43 (53 μM), and BC-ash9 (42 μM). The BC-ash0 generated only 8 μM of Fe(II) after 120 min. The higher Fe(II) formation potential of the ash-amended biochars is in line with their higher EDC values (Fig. 2b and Table S4). Ash amendments of 9 wt%, 16 wt%, and 43 wt% led to an 8-, 14-, and 5-fold increase in the EDC values of the biochars compared to BC-ash0 (Table S4). BC-ash16 possessed the highest EDC of 590 ± 12 μmol e$^-$ (g biochar)$^{-1}$ (Fig. 2b and Table S4). The increase in EDC was not linear with the amount of ash added, suggesting that there is an optimal amount of ash amendment to maximize the EDC of the biochar produced at 500 °C. The raw ash itself had a low EDC value of 53 μmol e$^-$ (g ash)$^{-1}$ [33], indicating that the ash alone was not responsible for the elevated EDC values of the ash-amended biochars. Additional redox-active moieties might have formed during pyrolysis in the presence of ash by catalyzing secondary charring reactions [50], contributing to the improved redox properties of these biochars.

3.2.2. Redox-active moieties governing the performance of ash-amended biochars

We further characterized the ash-amended biochars to gain a better understanding of which properties govern their performance in the biochar/Fe(III)/PDS system (Fig. 2d – f). The non-ash amended as well as the ash-amended softwood sawdust biochars showed PFR concentrations in the range of 10^{18} spins (g biochar)$^{-1}$ (Fig. 2e and Table S4). The PFR concentration decreased linearly ($R^2 = 0.99$) but only slightly with increasing ash amendment (Fig. 2e). The BC-ash0 mainly contained carbon-centered PFRs as indicated by a g-value of 2.0029 [44]. This finding is consistent with beech wood biochars, which had a similar final ash content (2.1 – 3.5 %, Table S2) than the BC-ash0 (2.3 % ash) and g-values of 2.0028 – 2.0029 (Table S4). For the ash-amended biochars, the g-values were in the range of 2.0030 – 2.0031 (Fig. 2e and Table S4) indicating carbon-centered radicals with an adjacent oxygen atom [44]. These results hint at a potential shift of redox-active PFRs from aryl radicals (carbon-centered) in non-ash amended biochars to semiquinone radicals (intermediate of the phenolic C-OH and quinoid C=O groups) in

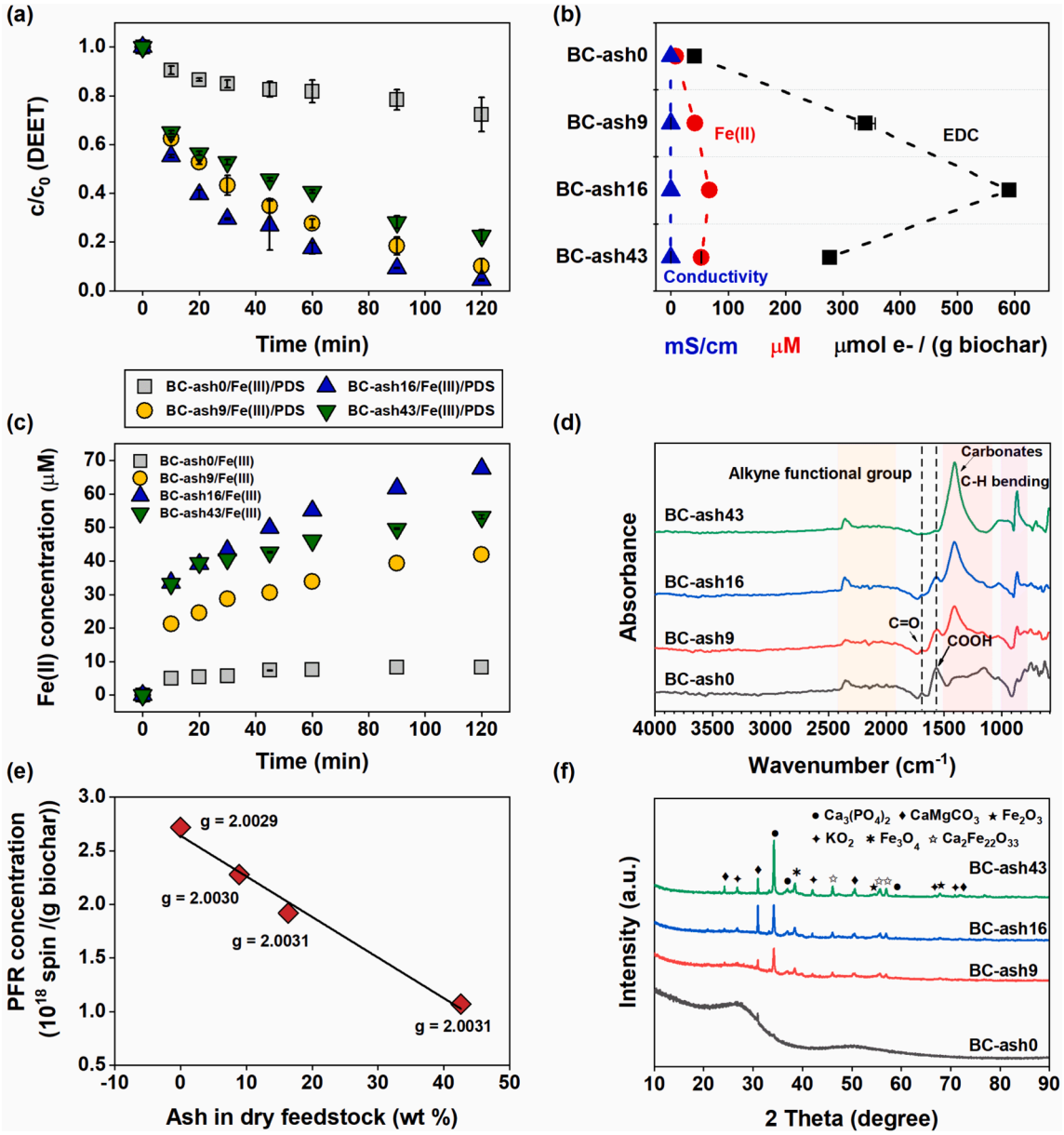

Fig. 2. (a) Kinetics of DEET transformation in the biochar/Fe(III)/PDS system with ash-amended biochars (BC-ash9, BC-ash16, and BC-ash43) and a non-ash amended control biochar (BC-ash0). [Biochar] = 1 g L^{-1}, [Fe(III)] = 0.2 mM, [PDS] = 8 mM, $[DEET]_0 = c_0 \sim 40$ μM after sorption equilibrium, c = measured DEET concentration over time, pH 2.5. Error bars indicate the standard deviation of triplicate experiments. (b) Electron donating capacity (EDC, E_h (MEO) = 0.61 V) and electrical conductivity (SEC, pressure 160 MPa) of BC-ash0, BC-ash9, BC-ash16, and BC-ash43, and corresponding Fe(II) formation after 120 min in biochar suspensions spiked with Fe(III). [Biochar] = 1 g L^{-1}, [Fe(III)] = 0.2 mM, pH 2.5. Error bars indicate the standard deviation of triplicate experiments. (c) Fe(II) formation in suspensions spiked with Fe(III). [Biochar] = 1 g L^{-1}, [Fe(III)] = 0.2 mM, pH 2.5. (d) ATR-FTIR spectra. (e) Correlation of persistent free radical (PFR) concentrations with weight percent of amended ash to dry feedstock during biochar pyrolysis ($R^2 = 0.99$). (f) X-ray diffraction (XRD) spectra of BC-ash0, BC-ash9, BC-ash16, and BC-ash43 with indicated formation of β-tricalcium phosphate ($Ca_3(PO_4)_2$), dolomite ($CaMgCO_3$), hematite (Fe_2O_3), potassium superoxide (KO_2), magnetite (Fe_3O_4), and calcium ferrites ($Ca_2Fe_{22}O_{33}$).

ash-amended biochars [18]. Such formation of semiquinone type radicals in ash-amended biochars may enhance Fe(III) reduction and PDS activation.

Even though all ash-amended biochars contained similar PFR concentrations and types, we observed differences in DEET transformation kinetics (Fig. 2a), which may be caused by different redox-active moieties such as oxygen functional groups or metals. FTIR measurements showed that electron donating oxygen functional groups, mainly –C=O and –COOH groups, decreased with increasing ash amendment, and were almost absent in BC-ash43 (Fig. 2d). The ash, which was added prior to pyrolysis, contained metals that can form redox-active crystalline minerals in the biochars during pyrolysis [32,51]. Indeed, the Fe and Mn contents of the biochars increased with increasing ash amendment (Table S1). The BC-ash43 had the highest Fe and Mn content of 178 μmol (g biochar)$^{-1}$ and 22 μmol (g biochar)$^{-1}$, respectively. These values are 28 times and 1.8 times higher than the Fe and Mn content of BC-ash0, respectively (Table S1). When calculating the contribution of these metal species to the EDCs in molar ratio, 64 % of the EDC of the BC-ash43 could be attributed to Fe, while for BC-ash16, BC-ash-9, and BC-ash0 the contribution of Fe was in a similar range of 16 % (Table S1). Metals in biochars usually occur as minerals [52]. XRD analysis showed pronounced differences in mineralogy of the biochars with and without ash amendment (Fig. 2f). BC-ash0 showed an amorphous profile with almost no peaks. In contrast, the ash-amended biochars showed distinct

signals, indicating the presence of ash-derived crystalline minerals. Hematite (Fe_2O_3) and magnetite (Fe_3O_4), two common redox-active iron minerals were observed in all ash-amended biochars (Fig. 2f). Magnetite, a mixed-valent iron [Fe(II)/Fe(III)] mineral, may exhibit higher Fe (III) reduction activity than hematite, an Fe(III)-bearing mineral, due to its ability to donate electrons *via* the Fe(II) sites [53,54]. The formation of redox-active Fe crystalline minerals in the ash-amended biochars likely contributed to the higher EDCs and enhanced Fe(III) reduction and PDS activation compared to the non-ash amended control biochar. Although the highest amount of crystalline iron minerals was formed in BC-ash43, their beneficial effect might be constrained by the low abundance of redox-active –C=O and –COOH functional groups (Fig. 2d) and lower PFR concentration (Fig. 2e), both mainly due to the lower carbon content of BC-ash43. We hypothesize that the good performance of BC-ash16 is due to the beneficial co-occurrence of redox-active moieties including crystalline Fe minerals (Fig. 2f), semiquinone radicals (Fig. 2e), and oxygen functional groups (e.g. –C=O and –COOH groups, Fig. 2d), which together lead to a high Fe(III) reduction (Fig. 2b and 2c) and subsequent PDS activation. These results indicate a complex interplay and potentially more pronounced role of redox-active oxygen functional groups and PFRs in ash-amended biochars.

All softwood sawdust biochars (BC-ash0, BC-ash9, BC-ash16, and BC-ash43) showed low SECs as they were produced at low pyrolysis temperature (500 °C), where conductive conjugated aromatic structures that can induce electron transfer were hardly formed, which is consistent with a relatively high H/C ratio of the biochars (0.25 – 0.47, Table S4). Altogether, the characterization of the softwood sawdust biochars with and without ash amendment demonstrated the contribution of oxygen functional groups and PFRs to their redox-active properties, which is consistent with the findings for beech wood biochars. Particularly, ash amendment led to the formation of redox-active crystalline iron minerals and semiquinoid persistent free radicals that promoted Fe(III) reduction and PDS activation in the biochar/Fe(III)/PDS system.

4. Conclusion

Biochar can facilitate electron transfer by redox-active surface moieties and/or bulk carbon matrices, which is greatly dependent on the biochar pyrolysis temperature. We showed that biochar derived at low pyrolysis temperature $\leq$ 600 °C is enriched with oxygen functional groups and PFRs that can reversibly accept and donate electrons. Low temperature biochars containing high amounts of oxygen functional groups and PFRs exhibited the best performance for DEET transformation in the presence of Fe(III) and persulfate. In contrast, high temperature biochars possessed a high content of conjugated aromatic structures and did not lead to DEET transformation, despite their ability to reduce Fe(III). Moreover, we showed that co-pyrolysis of biomass with wood ash, a widely available by-product of many bioenergy applications, enhanced the redox-active properties of biochars. This resulted in biochars with high EDCs that can efficiently be employed for DEET transformation in the biochar/Fe(III)/PDS system. Ash amendments of 16 wt% produced the best-performing biochar with high content of redox-active functional groups, PFRs, and ash-derived crystalline minerals. While our study showed that the characteristics and performance of the biochars depend on the amount of ash added, future work is needed to systematically investigate the combined effects of ash type and pyrolysis temperature. Future research should also look into the use of iron and/or earth alkali metal salts as defined mineral additives in biochar production to achieve similar effects.

Our study can inform the production of engineered biochars with redox-active properties tailored for different applications such as persulfate activation in the presence of Fe(III) for target contaminant removal from water. The production of biochars with high amounts of oxygen functional groups, PFRs, and redox-active minerals seems promising for enhancing the transformation of organic contaminants in heterogeneous persulfate-based oxidation processes, while high-temperature biochars were shown to be of lower relevance. Further research is needed to better understand the effects of feedstock treatments on the redox properties of biochars and their performance to degrade various organic contaminants. To use these highly complex carbonaceous materials for specific applications such as water treatment, future studies should investigate the long-term stability and performance as well as the reusability of biochars. Standardized biochar production procedures need to be continuously refined to ensure consistent biochar production with minimal risk of secondary pollution (i.e., biochar must not leach potentially toxic compounds). In addition, performance monitoring strategies are required to optimize the removal of target contaminants while minimizing the risk of potential transformation product formation. To tailor the application of the biochar/Fe(III)/PDS system in water treatment, future studies should also focus on elucidating the formation of reactive radical or nonradical species in different water matrices.

CRediT authorship contribution statement

Yiling Zhuang: Conceptualization, Methodology, Validation, Investigation, Formal analysis, Data curation, Writing – original draft, Visualization. **Stefan B. Haderlein:** Conceptualization, Resources, Methodology, Writing – review & editing, Supervision. **Nikolas Hagemann:** Resources, Methodology, Investigation, Writing – review & editing. **Jannis Grafmüller:** Investigation, Writing – review & editing. **Karolin Gogler:** Investigation, Writing – review & editing. **Andrea Paul:** Investigation, Writing – review & editing. **Friedrich Fink:** Investigation, Writing – review & editing. **Stephanie Spahr:** Conceptualization, Resources, Methodology, Data curation, Writing – original draft, Writing – review & editing, Supervision.

Declaration of competing interest

The authors declare that they have no known competing financial interests or personal relationships that could have appeared to influence the work reported in this paper.

Acknowledgements

This work was funded by the China Scholarship Council (CSC, File No. 201904910454). We thank Claudia Schmalsch for support in the laboratory, Marvin Sens and Christiane Herzog for analyzing the metal contents of the biochar samples.

Appendix A. Supplementary material

Supplementary data to this article can be found online at https://doi.org/10.1016/j.seppur.2025.133634.

Data availability

Data will be made available on request.

References

[1] L.W. Matzek, K.E. Carter, Activated persulfate for organic chemical degradation: a review, Chemosphere 151 (2016) 178–188.
[2] J. Lee, U. Von Gunten, J.-H. Kim, Persulfate-based advanced oxidation: critical assessment of opportunities and roadblocks, Environ. Sci. Tech. 54 (2020) 3064–3081.
[3] Z. Zhou, X. Liu, K. Sun, C. Lin, J. Ma, M. He, W. Ouyang, Persulfate-based advanced oxidation processes (AOPs) for organic-contaminated soil remediation: a review, Chem. Eng. J. 372 (2019) 836–851.
[4] L. Zhao, H. Hou, A. Fujii, M. Hosomi, F. Li, Degradation of 1,4-dioxane in water with heat-and Fe^{2+}-activated persulfate oxidation, Environ. Sci. Pollut. Res. 21 (2014) 7457–7465.

[5] S. Wang, J. Wu, X. Lu, W. Xu, Q. Gong, J. Ding, B. Dan, P. Xie, Removal of acetaminophen in the Fe^{2+}/persulfate system: kinetic model and degradation pathways, Chem. Eng. J. 358 (2019) 1091–1100.

[6] H. Luo, Y. Zeng, D. He, X. Pan, Application of iron-based materials in heterogeneous advanced oxidation processes for wastewater treatment: a review, Chem. Eng. J. 407 (2021) 127191.

[7] X. Pan, Z. Gu, W. Chen, Q. Li, Preparation of biochar and biochar composites and their application in a Fenton-like process for wastewater decontamination: a review, Sci. Total Environ. 754 (2021) 142104.

[8] D. Huang, H. Luo, C. Zhang, G. Zeng, C. Lai, M. Cheng, R. Wang, R. Deng, W. Xue, X. Gong, X. Guo, T. Li, Nonnegligible role of biomass types and its compositions on the formation of persistent free radicals in biochar: insight into the influences on Fenton-like process, Chem. Eng. J. 361 (2019) 353–363.

[9] H. Wang, W. Guo, R. Yin, J. Du, Q. Wu, H. Luo, B. Liu, F. Sseguya, N. Ren, Biochar-induced Fe(III) reduction for persulfate activation in sulfamethoxazole degradation: insight into the electron transfer, radical oxidation and degradation pathways, Chem. Eng. J. 362 (2019) 561–569.

[10] Y. Tang, J. Dou, Z. Lu, J. Xu, Y. He, Accelerating Fe^{2+}/Fe^{3+} cycle via biochar to improve catalytic degradation efficiency of the Fe^{3+}/persulfate oxidation, Environ. Pollut. 316 (2023) 120669.

[11] Y. Zhuang, S. Spahr, H.V. Lutze, C.J. Reith, N. Hagemann, A. Paul, S.B. Haderlein, Persulfate activation by biochar and iron: Effect of chloride on formation of reactive species and transformation of *N,N*-diethyl-*m*-toluamide (DEET), Water Res. 265 (2024) 122267.

[12] L. Zeng, Q. Chen, Y. Tan, P. Lan, D. Zhou, M. Wu, N. Liang, B. Pan, B. Xing, Dual roles of biochar redox property in mediating 2,4-dichlorophenol degradation in the presence of Fe^{3+} and persulfate, Chemosphere 279 (2021) 130456.

[13] J. Lu, Q. Lu, L. Di, Y. Zhou, Y. Zhou, Iron-based biochar as efficient persulfate activation catalyst for emerging pollutants removal: a review, Chin. Chem. Lett. 108357 (2023).

[14] J. Liang, X. Duan, X. Xu, K. Chen, F. Wu, H. Qiu, C. Liu, S. Wang, X. Cao, Biomass-derived pyrolytic carbons accelerated Fe(III)/Fe(II) redox cycle for persulfate activation: pyrolysis temperature-depended performance and mechanisms, Appl. Catal. B Environ. 297 (2021) 120446.

[15] R. Tian, H. Dong, J. Chen, R. Li, Q. Xie, L. Li, Y. Li, Z. Jin, S. Xiao, J. Xiao, Electrochemical behaviors of biochar materials during pollutant removal in wastewater: a review, Chem. Eng. J. 425 (2021) 130585.

[16] X. Li, H. Cao, Y. Cao, Y. Zhao, W. Zhang, J. Shen, Z. Sun, F. Ma, Q. Gu, Insights into the mechanism of persulfate activation with biochar composite loaded with Fe for 2,4-dinitrotoluene degradation, J. Environ. Manage. 341 (2023) 117955.

[17] F.J. Chacón, M.L. Cayuela, A. Roig, M.A. Sánchez-Monedero, Understanding, measuring and tuning the electrochemical properties of biochar for environmental applications, Rev. Environ. Sci. Biotechnol. 16 (2017) 695–715.

[18] F.J. Chacon, M.A. Sanchez-Monedero, L. Lezama, M.L. Cayuela, Enhancing biochar redox properties through feedstock selection, metal preloading and post-pyrolysis treatments, Chem. Eng. J. 395 (2020) 125100.

[19] S. Joseph, O. Husson, E.R. Graber, L. Van Zwieten, S. Taherymoosavi, T. Thomas, S. Nielsen, J. Ye, G. Pan, C. Chia, P. Munroe, J. Allen, Y. Lin, X. Fan, S. Donne, The electrochemical properties of biochars and how they affect soil redox properties and processes, Agronomy 5 (2015) 322–340.

[20] K. Luo, Y. Pang, D. Wang, X. Li, L. Wang, M. Lei, Q. Huang, Q. Yang, A critical review on the application of biochar in environmental pollution remediation: role of persistent free radicals (PFRs), J. Environ. Sci. 108 (2021) 201–216.

[21] L. Kemmou, Z. Frontistis, J. Vakros, I.D. Manariotis, D. Mantzavinos, Degradation of antibiotic sulfamethoxazole by biochar-activated persulfate: factors affecting the activation and degradation processes, Catal. Today 313 (2018) 128–133.

[22] G. Fang, C. Liu, J. Gao, D.D. Dionysiou, D. Zhou, Manipulation of persistent free radicals in biochar to activate persulfate for contaminant degradation, Environ. Sci. Tech. 49 (2015) 5645–5653.

[23] T. Sun, B.D. Levin, J.J. Guzman, A. Enders, D.A. Muller, L.T. Angenent, J. Lehmann, Rapid electron transfer by the carbon matrix in natural pyrogenic carbon, Nat. Commun. 8 (2017) 14873.

[24] L. Klüpfel, M. Keiluweit, M. Kleber, M. Sander, Redox properties of plant biomass-derived black carbon (biochar), Environ. Sci. Tech. 48 (2014) 5601–5611.

[25] Y. Zhang, X. Xu, L. Cao, Y.S. Ok, X. Cao, Characterization and quantification of electron donating capacity and its structure dependence in biochar derived from three waste biomasses, Chemosphere 211 (2018) 1073–1081.

[26] K. Weber, P. Quicker, Properties of biochar, Fuel 217 (2018) 240–261.

[27] L. Luo, C. Xu, Z. Chen, S. Zhang, Properties of biomass-derived biochars: combined effects of operating conditions and biomass types, Bioresour. Technol. 192 (2015) 83–89.

[28] J.A. Ippolito, L. Cui, C. Kammann, N. Wrage-Mönnig, J.M. Estavillo, T. Fuertes-Mendizabal, M.L. Cayuela, G. Sigua, J. Novak, K. Spokas, N. Borchard, Feedstock choice, pyrolysis temperature and type influence biochar characteristics: a comprehensive meta-data analysis review, Biochar 2 (2020) 421–438.

[29] M. Keiluweit, P.S. Nico, M.G. Johnson, M. Kleber, Dynamic molecular structure of plant biomass-derived black carbon (biochar), Environ. Sci. Tech. 44 (2010) 1247–1253.

[30] M. Kaltschmitt, H. Hartmann, H. Hofbauer. Energie aus Biomasse: Grundlagen, Techniken und Verfahren, Springer-Verlag Berlin Heidelberg, 2009.

[31] S. Cairns, S. Chaudhuri, G. Sigmund, I. Robertson, N. Hawkins, T. Dunlop, T. Hofmann, Wood ash amended biochar for the removal of lead, copper, zinc and cadmium from aqueous solution, Environ. Technol. Innov. 24 (2021) 101961.

[32] W. Wu, B. Yan, L. Zhong, R. Zhang, X. Guo, X. Cui, W. Lu, G. Chen, Combustion ash addition promotes the production of K-enriched biochar and K release characteristics, J. Clean. Prod. 311 (2021) 127557.

[33] J. Grafmüller, A. Böhm, Y. Zhuang, S. Spahr, P. Müller, T.N. Otto, T.D. Bucheli, J. Leifeld, R. Giger, M. Tobler, H.-P. Schmidt, N. Dahmen, N. Hagemann, Wood ash as an additive in biomass pyrolysis: effects on biochar yield, properties, and agricultural performance, ACS Sustain. Chem. Eng. 10 (2022) 2720–2729.

[34] R.M. Pitman, Wood ash use in forestry–a review of the environmental impacts, Forestry 79 (2006) 563–588.

[35] N. Hagemann, H.-P. Schmidt, R. Kägi, M. Böhler, G. Sigmund, A. Maccagnan, C. S. McArdell, T.D. Bucheli, Wood-based activated biochar to eliminate organic micropollutants from biologically treated wastewater, Sci. Total Environ. 730 (2020) 138417.

[36] S.V. Vassilev, D. Baxter, L.K. Andersen, C.G. Vassileva, An overview of the chemical composition of biomass, Fuel 89 (2010) 913–933.

[37] S.V. Vassilev, D. Baxter, L.K. Andersen, C.G. Vassileva, An overview of the composition and application of biomass ash. Part 1. Phase–mineral and chemical composition and classification, Fuel 105 (2013) 40–76.

[38] L.L. Stookey, Ferrozine—a new spectrophotometric reagent for iron, Anal. Chem. 42 (1970) 779–781.

[39] K. Amstaetter, T. Borch, A. Kappler, Influence of humic acid imposed changes of ferrihydrite aggregation on microbial Fe (III) reduction, Geochim. Cosmochim. Acta 85 (2012) 326–341.

[40] Umwelt-Ost. Eurofins. Conductivity meter Black Gauss I - technical documentation. Zenodo, 2023, https://doi.org/10.5281/zenodo.8197758.

[41] EBC (2012-2023) European Biochar Certificate - Guidelines for a Sustainable Production of Biochar. Carbon Standards International (CSI), Frick, Switzerland. (http://european-biochar.org). Version 10.3 from 5th Apr 2022.

[42] Q.-F. Zheng, Y.-H. Wang, Y.-G. Sun, H.-H. Niu, J.-R. Zhou, Z.-M. Wang, J. Zhao, Study on structural properties of biochar under different materials and carbonized by FTIR, Spectrosc. Spectr. Anal. 34 (2014) 962–966.

[43] J. Yuan, Y. Wen, D.D. Dionysiou, V.K. Sharma, X. Ma, Biochar as a novel carbon-negative electron source and mediator: electron exchange capacity (EEC) and environmentally persistent free radicals (EPFRs): a review, Chem. Eng. J. 429 (2022) 132313.

[44] H. Von Bardeleben, J. Cantin, A. Zeinert, B. Racine, K. Zellama, P. Hai, Spins and microstructure of hydrogenated amorphous carbon: a multiple frequency electron paramagnetic resonance study, Appl. Phys. Lett. 78 (2001) 2843–2845.

[45] J. Qin, Q. Chen, M. Sun, P. Sun, G. Shen, Pyrolysis temperature-induced changes in the catalytic characteristics of rice husk-derived biochar during 1,3-dichloropropene degradation, Chem. Eng. J. 330 (2017) 804–812.

[46] W. Xu, J.J. Pignatello, W.A. Mitch, Role of black carbon electrical conductivity in mediating hexahydro-1,3,5-trinitro-1,3,5-triazine (RDX) transformation on carbon surfaces by sulfides, Environ. Sci. Tech. 47 (2013) 7129–7136.

[47] W. Ren, G. Nie, P. Zhou, H. Zhang, X. Duan, S. Wang, The intrinsic nature of persulfate activation and N-doping in carbocatalysis, Environ. Sci. Tech. 54 (2020) 6438–6447.

[48] J. Dou, Y. Tang, Z. Lu, G. He, J. Xu, Y. He, Neglected but efficient electron utilization driven by biochar-coactivated phenols and peroxydisulfate: polyphenol accumulation rather than mineralization, Environ. Sci. Tech. 57 (2023) 5703–5713.

[49] W. Ren, C. Cheng, P. Shao, X. Luo, H. Zhang, S. Wang, X. Duan, Origins of electron-transfer regime in persulfate-based nonradical oxidation processes, Environ. Sci. Tech. 56 (2021) 78–97.

[50] A. Anca-Couce, Reaction mechanisms and multi-scale modelling of lignocellulosic biomass pyrolysis, Prog. Energy Combust. Sci. 53 (2016) 41–79.

[51] W. Buss, S. Jansson, O. Mašek, Unexplored potential of novel biochar-ash composites for use as organo-mineral fertilizers, J. Clean. Prod. 208 (2019) 960–967.

[52] S. Joseph, E. Graber, C. Chia, P. Munroe, S. Donne, T. Thomas, S. Nielsen, C. Marjo, H. Rutlidge, G.-X. Pan, L. Li, P. Taylor, A. Rawal, J. Hook, Shifting paradigms: development of high-efficiency biochar fertilizers based on nano-structures and soluble components, Carbon Manag. 4 (2013) 323–343.

[53] C. Zhang, L. Li, Z. Yuan, X. Xu, Z. Song, Y.R. Zhang, Mechanical properties of siderite and hematite from DFT calculation, Miner. Eng. 146 (2020) 106107.

[54] G. Wen, J.-W. Li, A.H. Hofstra, A.E. Koenig, H.A. Lowers, D. Adams, Hydrothermal reequilibration of igneous magnetite in altered granitic plutons and its implications for magnetite classification schemes: insights from the Handan-Xingtai iron district, North China Craton, Geochim. Cosmochim. Acta 213 (2017) 255–270.